Communicating with Large Intelligent Surfaces: Fundamental Limits and Models

(Article begins on next page)

Communicating with Large Intelligent Surfaces: Fundamental Limits and Models

Davide Dardari, *Senior Member, IEEE*

Abstract—This paper analyzes the optimal communication involving large intelligent surfaces (LIS) starting from electromagnetic arguments. Since the numerical solution of the corresponding eigenfunctions problem is in general computationally prohibitive, simple but accurate analytical expressions for the link gain and available spatial degrees-of-freedom (DoF) are derived. It is shown that the achievable DoF and gain offered by the wireless link are determined only by geometric factors, and that the classical Friis' formula is no longer valid in this scenario where the transmitter and receiver could operate in the near-field regime. Furthermore, results indicate that, contrarily to classical MIMO systems, when using LIS-based antennas DoF larger than 1 can be exploited even in strong line-of-sight (LOS) channel conditions, which corresponds to a significant increase in spatial capacity density, especially when working at millimeter waves.

Index Terms—Large intelligent surfaces; metasurfaces; holographic MIMO; wireless communication; fundamental limits; degrees of freedom

Fig. 1. Example of LIS-based communication scenario.

I. INTRODUCTION

FUTURE wireless networks are expected to become distributed intelligent communication, sensing and computing entities. This will allow to meet ultra-reliability, high capacity densities, extremely low-latency and low-energy consumption requirements posed by emerging application scenarios such as Industrial Internet of Things in Factories of the Future [1], [2]. The current trend in satisfying part of such requirements is through cell densification, massive multiple-input multiple-output (MIMO) transmission, and the exploitation of higher frequency bands (e.g., millimeter and THz) [3], [4]. Unfortunately, when moving to higher frequency bands the channel path-loss increases and the multipath becomes sparse so that the spatial multiplexing peculiarity of MIMO, i.e., the channel degrees-of-fredom (DoF), guaranteed at lower frequencies by rich multipath, is lost in favor of only beamforming gain which increases the communication capacity logarithmically instead of linearly with the number of antennas [5].

The introduction of metamaterials to realize, for instance, the so called *metasurfaces* [6]–[8], has attracted a wide interest in different research communities with applications including transmitarrays [9], metamirrors [10]–[12], reflectarrays [13], [14], metaprisms [15], and holograms [7], [16]. Furthermore, the recent development of programmable metasurfaces, used as smart electromagnetic (e.m.) reflectors and large configurable antennas, has opened new very appealing perspectives [9], [17]–[20]. In fact, these *intelligent surfaces* can be easily
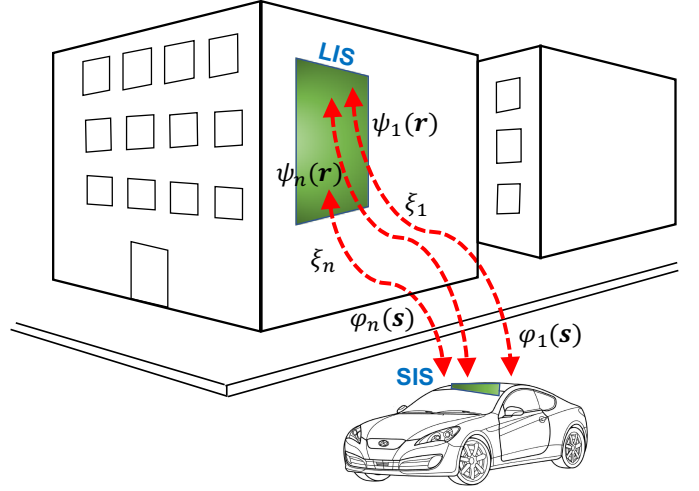
D. Dardari is with the Dipartimento di Ingegneria dell'Energia Elettrica e dell'Informazione "Guglielmo Marconi" (DEI), CNIT, University of Bologna, Cesena Campus, Cesena (FC), Italy, (e-mail: davide.dardari@unibo.it).

embedded in daily life objects such as walls, clothes, buildings, etc.. Environments coated with intelligent surfaces constitute the recently proposed *smart radio environments* concept [21]–[23]. In smart radio environments, the design paradigm is changed from wireless devices/networks that adapt themselves to the environment (e.g., propagation conditions), to the joint optimization of both devices and environment using reconfigurable intelligent surfaces (RISs).

The advantages of RIS-enabled systems have been analyzed in several papers. For instance, in [24] a RIS-enhanced orthogonal frequency division multiplexing (OFDM) system is investigated, where the power allocation and the phase profile of the metasurface are jointly optimized to boost the achievable rate of a cell-edge user. In [25], [26], it is shown that the channel rank of MIMO communication in line-of-sight (LOS) can be increased by adding a RIS generating an artificial path that can be exploited by the MIMO system to increase the capacity. The authors in [27] present a comparison between RIS- and relay-enabled wireless networks by discussing the similarities and differences. Other studies can be found, for instance, in [28], [29]. An interesting alternative to RISs is given by *metaprisms*, which are passive and non-configurable frequency-selective metasurfaces proposed in [15]. With an appropriate design of the metaprism, it is possible to control that each data stream in an OFDM system is reflected to the desired direction by properly dispatching subcarriers to users. This helps to cover areas experiencing severe non line-of-sight (NLOS) channel conditions at low-cost.

A. Related Work

Most of the papers dealing with intelligent surfaces, such as those cited above, use them as (possibly reconfigurable) reflectors to assist multipath propagation. A few papers analyze the potential of using metasurfaces as large antennas, namely large intelligent surface (LIS)-based antennas, to improve the communication capacity [18], [20], [30] or to enable single-anchor localization [31].

One question is whether smart metasurfaces can be used as the enabling technology to approach the full control of e.m. waves generated or sensed by antennas. In fact, with metamaterials e.m. waves can be shaped almost arbitrarily, at least in theory. It is expected that this unprecedented flexibility offered by LISs (e.g., on walls), or medium intelligent surfaces (MISs) (e.g., on cars/truck), and small intelligent surfaces (SISs) (e.g., on smartphones/sensors), will provide a great opportunity to move towards the ultimate capacity limit of the wireless channel.

The main fundamental results on the physical limitation brought by the e.m. transportation of information can be found in [32]–[35] and references therein. The authors in [36] extend these results by generalizing the Clarke's channel model to non-isotropic random scattering environments using a mathematically tractable framework based on Fourier plane-wave series expansion of the channel. With this model they show that the DoF of the e.m. wave on a continuous large antenna aperture is proportional to the surface area normalized to the square wavelength [37]. These results mainly address the computation of the spatial dimensionality of the e.m. field when considering finite volumes with sources and scatterers in the far-field, but they do not consider the spatial DoF available in a communication system employing intelligent surfaces as transmit and receive antennas, possibly in the near-field region.

The adoption of LIS-enabled antennas provides high flexibility in network design as well as the potential to achieve the goals of next generation wireless networks, but it has also opened several fundamental questions that are still unsolved, such as understanding the theoretical limits and how to achieve them in practice.

With LISs, classical models for antenna arrays fail to capture the actual wireless link characteristics in terms of gain, path-loss and available DoF as they assume (Fraunhofer) far-field condition (i.e., a distance much larger than the antenna dimension so that waves can be considered plane [38]), whereas with LISs the size of the antenna becomes comparable to the distance of the link (near-field regime). Moreover, they usually do not account for the flexibility in generating the current distribution offered by LISs (holographic capability) and hence common results of aperture antennas are no longer valid. Therefore, new models based on the ultimate physical limitation brought by the e.m. transportation of information should be considered.

One of the earliest works proposing and studying LISs for communication is [30], which considers the communication between a single-antenna user with a LIS, where an analysis of the spatial capacity density is presented. Practical aspects related to the design of the optimal sampling lattice of the LIS

are considered by showing that the hexagonal lattice is optimal for minimizing the surface's area of a LIS under the constraint that one independent signal dimension should be obtained per spent antenna element of the LIS.

The work has been extended in [39] by the same authors to investigate the optimal user assignments for a distributed LIS system with several LIS units, with the purpose to select the set of best units to serve a given number of users simultaneously. The multi-user scenario is considered also in [40], where it is shown that when using a massive MIMO system with extremely large arrays, users can effectively communicate only with a sub-part of the array, thus creating non-stationary patterns. The paper proposes a receiver architecture based on subarray processing capable of dealing with this situation.

In [41], the distribution of the sum-rate of an uplink LIS network under imperfect channel estimation is investigated through an asymptotic analysis, from which expressions for the outage probability are derived and used to show that LIS-based systems can provide reliable communications. Further results can be found in the recent paper [42] published by the same authors, where the occurrence of channel hardening effects is also analyzed.

In [43] a general theory of space-time modulated digital coding metasurfaces to obtain simultaneous manipulations of e.m. waves in both space and frequency domains is proposed and validated in the far-field regime.

Finally, the issue of power and cost of large massive MIMO systems using metasurfaces is addressed in [20]. Such challenges are tackled by incorporating signal processing methods, such as compression and analog combining, in the physical antenna structure. The characterization of the maximal achievable sum-rate on the uplink and potential gain over standard antenna arrays are studied.

B. Main Contribution

To the author's knowledge, no results are present related to the investigation of the available spatial DoF as well as the coupling gain between intelligent surfaces, in particular when the maximum degree of flexibility in e.m. shaping is allowed, and one of the antennas is large so that it might operate in the near-field even at practical distances.

In this paper, the optimal communication between LIS/SIS is addressed as an eigenfunctions problem starting from an e.m. formulation, similarly to what done in [44], [45] for optical systems, and preliminarily addressed in [46]. Unfortunately, finding the solution to the eigenfunctions problem requires extensive and sometimes prohibitive e.m.-level simulations if large surfaces are considered, and usually they do not provide general insights. Therefore, we focus on obtaining approximate but accurate analytical expressions for the link gain and the available orthogonal communication channels (i.e., the DoF) between the transmitter and receiver. Although such expressions are easy to compute numerically, we further derive closed-form asymptotic and non-asymptotic expressions for some specific cases of interest which allow to get important insights about the communication between intelligent surfaces and can serve as design guidelines in future wireless networks employing LISs.

Furthermore, we show that, contrarily to classical MIMO, with LIS-based antennas the available DoF can be higher than 1, even in LOS channel condition, thus boosting in principle the channel capacity. This is useful when moving towards high frequencies where LOS communication becomes predominant and the multipath weaker so that conventional MIMO systems cannot benefit from multiplexing gain (i.e., the DoF), usually obtained by exploiting the multipath. In addition, the achievable DoF and gain offered by the wireless link are shown to be determined only by geometric factors normalized to the wavelength, and that the classical Friis' formula is no longer valid when using LISs. Asymptotic expressions for very large LISs or large distances put in evidence the difference between classical and LIS-based communication systems.

The remainder of this paper is organized as follows. In Section II, the general problem formulation is given. Analytical expressions for the link gain and the communication DoF for the general case as well as for same particular geometric configurations are derived, respectively, in Sections III and IV. Numerical results and discussions are presented in Section V. Finally, conclusions are given in Section. VI.

C. Notation and Definitions

Lowercase bold variables denote vectors in the 3D space, i.e., $\mathbf{r} = \mathbf{u}_x \cdot r_x + \mathbf{u}_y \cdot r_y + \mathbf{u}_z \cdot r_z$ is a vector with cartesian coordinates (r_x, r_y, r_z), $\hat{\mathbf{r}}$ is a unit vector denoting its direction, and $r = |\mathbf{r}|$ denotes its magnitude, where $\hat{\mathbf{u}}_x$, $\hat{\mathbf{u}}_y$ and $\hat{\mathbf{u}}_z$ represent the unit vectors in the x, y and z directions, respectively. Italic capital letters (e.g., $E(\mathbf{r})$, $J(\mathbf{r})$) represent electromagnetic vector functions. Boldface capital letters are matrices (e.g., $\mathbf{H}$), where $\mathbf{I}$ is the identity matrix, and † indicates the conjugate transpose operator. $\nabla^2 J(\mathbf{r})$ is the Laplacian of the vector function $J(\mathbf{r})$, whereas $\nabla \Phi$ and $\nabla \cdot J(\mathbf{r})$ are the gradient and divergence operators, respectively. Surfaces and volumes are indicated with calligraphic letters $\mathcal{S}_T$, where $A_T = |\mathcal{S}_T|$ is their Lebesgue measure. Define the $\mathcal{L}_2$-norm $||\mathbf{r}||$, the Frobenius norm $||\mathbf{X}|| = \sqrt{\sum_{k=1}^{N} \sum_{j=1}^{N} |\{\mathbf{X}\}_{kj}|^2}$, and the outer product (tensor product) $\mathbf{r} \otimes \mathbf{s}$, where $\{\mathbf{r} \otimes \mathbf{s}\}_{kj} = r_k s_j$, and $\{\mathbf{X}\}_{kj}$ is the kjth element of matrix $\mathbf{X}$. The notation $\mathbb{L}^2(\mathcal{S}_T)$ indicates the Hilbert space corresponding to the square-integrable functions defined on $\mathcal{S}_T$. Furthermore, denote with μ, ϵ, and $\eta = \sqrt{\mu/\epsilon}$ the permittivity, permeability and impedance of free-space, respectively, and c the speed-of-light.

II. GENERAL PROBLEM FORMULATION

Thanks to the adoption of metamaterials, with LISs one can synthesize in principle any current distribution, then it is of interest to investigate how many orthogonal channels, i.e., DoF, can be established when two LIS/SIS are communicating with each other. To this purpose, we approximate the intelligent surface as a continuous array of an infinite number of infinitesimal antennas. A system having an uncountably infinite number of antennas in a finite space has been recently dubbed as *Holographic MIMO* [36].

A. Problem Formulation

Consider a transmit LIS or MIS/SIS antenna with surface $\mathcal{S}_T$ of area $A_T = |\mathcal{S}_T|$ containing e.m. monochromatic source currents with Fourier representation $J(\mathbf{s}, \omega)$ different from zero in $\mathbf{s} \in \mathcal{S}_T$, with ω being the angular frequency, which generate an electric field $E(\mathbf{r}, \omega)$ at the generic location $\mathbf{r}$ in free-space. Furthermore, we consider a receive LIS antenna $\mathcal{S}_R$ not intersecting $\mathcal{S}_T$, with area $A_R = |\mathcal{S}_R|$.[1] Due to the reciprocity of the radio medium, their role can be exchanged.

Each frequency component satisfies the inhomogeneous Helmholtz wave equation[2]

$$\nabla^2 E(\mathbf{r}) + k_0^2 E(\mathbf{r}) = \jmath k_0 \eta J(\mathbf{r}), \tag{1}$$

where $k_0 = \omega/c = 2\pi/\lambda$ is the wavenumber, λ the wavelength, and we have dropped the explicit dependence on ω to lighten the notation.

Any point source in $\mathcal{S}_T$ generates the (outgoing) wave given by the tensor Green's function [38]

$$G(\mathbf{r}) = -\frac{\jmath \omega \mu}{4\pi} \left[\mathbf{I} + \frac{1}{k_0} \nabla \nabla \right] \frac{\exp(-\jmath k_0 r)}{r}, \tag{2}$$

with $r = |\mathbf{r}|$, which obeys the Helmholtz equation.

By expanding (2) we obtain [48]

$$G(\mathbf{r}) = -\frac{\jmath \eta \exp(-\jmath k_0 r)}{2\lambda r} \left[\left(\mathbf{I} - \hat{\mathbf{r}} \cdot \hat{\mathbf{r}}^\dagger \right) + \frac{\jmath \lambda}{2\pi r} \left(\mathbf{I} - 3\,\hat{\mathbf{r}} \cdot \hat{\mathbf{r}}^\dagger \right) \right.$$

$$\left. -\frac{\lambda^2}{(2\pi r)^2} \left(\mathbf{I} - 3\,\hat{\mathbf{r}} \cdot \hat{\mathbf{r}}^\dagger \right) \right] \simeq -\frac{\jmath \eta \exp(-\jmath k_0 r)}{2\lambda r} \left(\mathbf{I} - \hat{\mathbf{r}} \cdot \hat{\mathbf{r}}^\dagger \right), \tag{3}$$

where we grouped the terms multiplying, respectively, the factors $1/r$, $1/r^2$ and $1/r^3$. It is evident from (3) that when $r \gg \lambda$, the second and third terms can be neglected and hence the right-hand side approximation in (3) holds.[3] By adding all the waves from the sources in $\mathcal{S}_T$, the resulting wave in $\mathbf{r}$ is

$$E(\mathbf{r}) = \int_{\mathcal{S}_T} G(\mathbf{r} - \mathbf{s}) J(\mathbf{s}) \, d\mathbf{s}. \tag{4}$$

The goal is to determine how many orthogonal communication channels, namely *communication modes*, with as large coupling intensities as possible can be activated between $\mathcal{S}_T$ and $\mathcal{S}_R$. This is associated to the optimal approximation of every element in the image space of a Hilbert-Schmidt operator in terms of singular functions. Specifically, define $\mathcal{X} = \mathbb{L}^2(\mathcal{S}_T)$ and $\mathcal{Y} = \mathbb{L}^2(\mathcal{S}_R)$ the Hilbert spaces corresponding to the square-integrable functions defined in $\mathcal{S}_T$ and $\mathcal{S}_R$, respectively. The function $E(\mathbf{r}) \in \mathcal{Y}$ can be seen as the image of $J(\mathbf{s}) \in \mathcal{X}$ through the Hilbert-Schmidt kernel $G(\mathbf{r}, \mathbf{s}) = G(\mathbf{r} - \mathbf{s})$ on $\mathcal{S}_T \times \mathcal{S}_R$, which induces the operator $G : \mathcal{X} \to \mathcal{Y}$ such that, for any $J \in \mathcal{X}$,

$$(G J)(\mathbf{r}) = \int_{\mathcal{S}_T} G(\mathbf{r}, \mathbf{s}) J(\mathbf{s}) \, d\mathbf{s}. \tag{5}$$

[1]Here we consider only surfaces because of their higher practical relevance, even though most of the following results can be extended to volumes as well.

[2]Similar formulation can be done for the magnetic field in case of magnetic currents even though it is always possible to model the problem using equivalent source currents [47].

[3]Under this condition the system does not work in the 'reactive' near-field.

Define the following self-adjoint Hilbert-Schmidt operators $G^\dagger G$ and $GG^\dagger$, with symmetric kernels

$$K_\mathrm{T}(\mathbf{s}, \mathbf{s}') = \int_{\mathcal{S}_\mathrm{R}} G^\dagger(\mathbf{r} - \mathbf{s}) \, G(\mathbf{r} - \mathbf{s}') \, d\mathbf{r} \tag{6}$$

$$K_\mathrm{R}(\mathbf{r}, \mathbf{r}') = \int_{\mathcal{S}_\mathrm{T}} G(\mathbf{r} - \mathbf{s}) \, G^\dagger(\mathbf{r}' - \mathbf{s}) \, d\mathbf{s}. \tag{7}$$

A fundamental property of Hilbert-Schmidt operators is that they are compact and admit either a finite or countably infinite orthonormal basis. In particular, two sets of orthonormal eigenfunctions $\{\phi_n(\mathbf{r})\}$, $\{\psi_n(\mathbf{s})\}$ exist, which are solutions, respectively, of the following coupled eigenfunction problems:

$$\xi^2 J(\mathbf{s}) = \int_{\mathcal{S}_\mathrm{T}} K_\mathrm{T}(\mathbf{s}, \mathbf{s}') J(\mathbf{s}') \, d\mathbf{s}' \tag{8}$$

$$\xi^2 E(\mathbf{r}) = \int_{\mathcal{S}_\mathrm{R}} K_\mathrm{R}(\mathbf{r}, \mathbf{r}') E(\mathbf{r}') \, d\mathbf{r}', \tag{9}$$

with the same real eigenvalues $\xi_1^2 \geq \xi_2^2 \geq \xi_3^2 \ldots$ [35], [49]. Note that $\{\phi_n(\mathbf{r})\}$ and $\{\psi_n(\mathbf{r})\}$ are two sets of orthonormal (vector) functions that are complete, respectively, in $\mathcal{S}_\mathrm{T}$ and $\mathcal{S}_\mathrm{R}$, i.e.,

$$\int_{\mathcal{S}_\mathrm{T}} \phi_n(\mathbf{r}) \, \phi_m^\dagger(\mathbf{r}) \, d\mathbf{r} = \delta_{nm} \qquad \int_{\mathcal{S}_\mathrm{R}} \psi_n(\mathbf{r}) \, \psi_m^\dagger(\mathbf{r}) \, d\mathbf{r} = \delta_{nm}, \tag{10}$$

being δ_{nm} the Kronecker delta.

As a consequence, any current density and wave in $\mathcal{S}_\mathrm{T}$ and $\mathcal{S}_\mathrm{R}$ can be written, respectively, as

$$J(\mathbf{r}) = \sum_n a_n \, \phi_n(\mathbf{r}) \qquad E(\mathbf{r}) = \sum_n b_n \, \psi_n(\mathbf{r}), \tag{11}$$

being a_n and b_n the inner products, respectively, of $J(\mathbf{r})$ and $\phi_n(\mathbf{r})$, and of $E(\mathbf{r})$ and $\psi_n(\mathbf{r})$. It can be easily verified that $b_n = \xi_n a_n$.

Consider now the following approximation of the kernel G in terms of D singular functions

$$G_D(\mathbf{r}, \mathbf{s}) = \sum_{n=1}^{D} \lambda_n u_n(\mathbf{r}) \otimes v_n^\dagger(\mathbf{s}). \tag{12}$$

For a fixed D, the best approximation of $G(\mathbf{r}, \mathbf{s})$ is obtained by choosing in (12) $u_n(\mathbf{r}) = \psi_n(\mathbf{r})$, $v_n(\mathbf{s}) = \phi_n(\mathbf{s})$, and $\lambda_n = \xi_n$, $n = 1, 2, \ldots D$, so that the error

$$e_D = \int_{\mathcal{S}_\mathrm{T}} \int_{\mathcal{S}_\mathrm{R}} ||G(\mathbf{r}, \mathbf{s}) - G_D(\mathbf{r}, \mathbf{s})||^2 \, d\mathbf{r} \, d\mathbf{s} = \sum_{n=D+1}^{\infty} \xi_n^2 \tag{13}$$

is minimized. This implies an optimal D-dimensional approximation of any function in $\mathcal{Y}$, image of the operator induced by the kernel G.

Since $\xi_D \to 0$, it is possible to optimally approximate the current density and wave, respectively, in $\mathcal{S}_\mathrm{T}$ and $\mathcal{S}_\mathrm{R}$, using (11) up to the first D terms with an error associated with the approximation at any level of accuracy.

The geometric interpretation of this result is that the generic source current $J(\mathbf{s})$ can be projected onto the coordinate system determined by the orthogonal (vector) eigenfunctions $\{\phi_n(\mathbf{s})\}$ then, through the kernel (or tensor) $G(\mathbf{r})$ in (4), the nth eigenfunction $\phi_n(\mathbf{s})$ of surface $\mathcal{S}_\mathrm{T}$ is put in one-to-one correspondence with the nth eigenfunction $\psi_n(\mathbf{r})$ of the receive
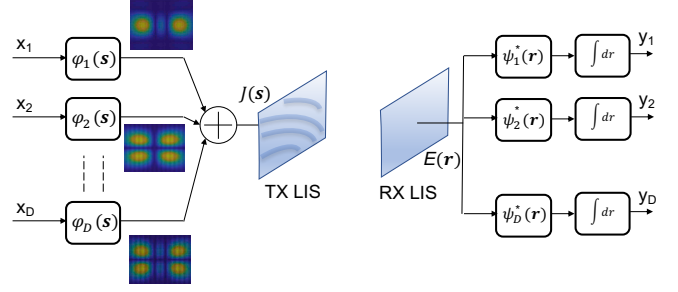

Fig. 2. Communication architecture based on orthogonal parallel channels.

surface $\mathcal{S}_\mathrm{R}$ through the scaling singular value ξ_n. Therefore, if one takes as source function the nth eigenfunction, i.e., $J(\mathbf{s}) = \phi_n(\mathbf{s})$, $\mathbf{s} \in \mathcal{S}_\mathrm{T}$, then the output electric field results $\xi_n \psi_n(\mathbf{r})$, $\mathbf{r} \in \mathcal{S}_\mathrm{R}$.

The eigenfunction decomposition ensures that the current distribution $\phi_1(\mathbf{s})$ in $\mathcal{S}_\mathrm{T}$ leads to the electric field $\xi_1 \psi_1(\mathbf{r})$ within $\mathcal{S}_\mathrm{R}$ with the largest intensity (eigenvalue ξ_1^2). The current distribution $\phi_2(\mathbf{s})$ in $\mathcal{S}_\mathrm{T}$ leads to the electric field $\xi_2 \psi_2(\mathbf{r})$ within $\mathcal{S}_\mathrm{R}$, orthogonal to $\xi_1 \psi_1(\mathbf{r})$, with the second largest intensity (eigenvalue ξ_2^2), and so on. Each pair of functions $(\phi_n(\mathbf{s}), \psi_n(\mathbf{r}))$ determines a spatial dimension of the system (*communication mode*) across which one can establish an orthogonal communication (see Fig. 1).

It is worth to point out that since in general the number of eigenvalues in the coupled eigenfunction problems (8) is infinity, the number of communication modes, namely the DoF, is defined conventionally as the minimum number D of eigenvalues sufficient to describe the signals within a given level of accuracy, e.g., compared to the noise intensity. A large level of coupling means that the generated wave is confined approximatively within the space between $\mathcal{S}_\mathrm{T}$ and $\mathcal{S}_\mathrm{R}$. Instead, a low level of coupling denotes that the generated wave is mainly dispersed away from the receiver's surface $\mathcal{S}_\mathrm{R}$.

By contrast, in MIMO systems the DoF corresponds to the rank of the channel matrix which is always no larger than the minimum between the number of transmit and receive antennas.

In terms of communication system representation, the eigenfunction decomposition leads to the optimal communication architecture depicted in Fig. 2. From it we obtain the input-output representation in terms of D parallel channels

$$y_n = \xi_n x_n + w_n, \quad n = 1, 2, \ldots, D, \tag{14}$$

being w_n the additive white Gaussian noise (AWGN), where the D input data streams $\{x_n\}$ are associated to the basis functions $\{\phi_n(s)\}$ in $\mathcal{S}_\mathrm{T}$ (i.e., current spatial distribution on the transmit surface), and they are recovered at the receiver after the correlation of the received signal $E(\mathbf{r})$ with the corresponding basis functions $\{\psi_n(\mathbf{s})\}$ in $\mathcal{S}_\mathrm{R}$. This scheme is information-theoretical optimal.

It is worthwhile to highlight that the capacity gain with respect to the case where $D = 1$, for a given signal-to-noise ratio (SNR), could be significant. For example, supposing

uniform power allocation among the D parallel channels, such gain is

$$G_C = \frac{D \log_2\left(1 + \frac{\text{SNR}}{D}\right)}{\log_2\left(1 + \text{SNR}\right)}, \qquad (15)$$

which increases with D.

B. Maximum Coupling Intensity Between Intelligent Surfaces

The effect of each polarization direction can be studied separately if the components of $J(\mathbf{s}) = J_x(\mathbf{s})\,\hat{\mathbf{u}}_x + J_y(\mathbf{s})\,\hat{\mathbf{u}}_y + J_z(\mathbf{s})\,\hat{\mathbf{u}}_z$ are taken orthogonal. Therefore, without loss of generality, suppose we excite the x-component, i.e., $J(\mathbf{s}) = J_x(\mathbf{s})\,\hat{\mathbf{u}}_x$. By exploiting the identity (37) in Appendix A and considering the last term of (3), the total normalized (i.e., dimensionless) coupling intensity between intelligent surfaces results

$$c_x = \frac{(4\pi)^2}{\lambda^2} \frac{1}{(\omega\mu)^2} \sum_n \xi_n^2 = \frac{4}{\eta^2} \int_{\mathcal{S}_R} \int_{\mathcal{S}_T} \|G_x(\mathbf{r} - \mathbf{s})\|^2 \, d\mathbf{r}\, d\mathbf{s}$$

$$= \frac{1}{\lambda^2} \int_{\mathcal{S}_R} \int_{\mathcal{S}_T} \frac{(r_y - s_y)^2 + (r_z - s_z)^2}{|\mathbf{r} - \mathbf{s}|^4} \, d\mathbf{r}\, d\mathbf{s}, \qquad (16)$$

where $\mathbf{r} = (r_x, r_y, r_z) \in \mathcal{S}_R$ and $\mathbf{s} = (s_x, s_y, s_z) \in \mathcal{S}_T$ represent the coordinates of the generic points on the receive and transmit surfaces, respectively.

The notation $G_x(\cdot)$ indicates we consider only the first column of tensor $G(\cdot)$, corresponding to the contribution caused by an excitation in the x-direction. Note that in general the excitation in the x-direction might contribute to all directions in the received electric field. The expressions for the other exciting directions are similars with mutual exchange of x, y and z.

In [44] the approximate solution to the eigenfunction problems valid for two collinear rectangular prisms at distance d, oriented along the z-axis, of volume $V_T = \Delta x_T\, \Delta y_T\, \Delta z_T$ and $V_R = \Delta x_R\, \Delta y_R\, \Delta z_R$, respectively, is presented. Specifically, the solution holds when the volumes are far apart compared to their sizes, i.e., $d \gg \Delta x_T, \Delta y_T, \Delta z_T, \Delta x_R, \Delta y_R, \Delta z_R$, which means they are in the (Fraunhofer) far-field region. In this case, the DoF available for communication has been found to be

$$D = \frac{\Delta x_T\, \Delta y_T \Delta x_R\, \Delta y_R}{d^2 \lambda^2}, \qquad (17)$$

whereas the total (un-normalized) coupling factor is

$$c = \frac{V_T\, V_R}{(4\pi d)^2}. \qquad (18)$$

Note that the thickness of volumes in the z axis does not affect the DoF but only the coupling intensity.

Incidentally, for very small antennas, i.e., $\Delta x_T \Delta x_R \ll \lambda\, d$, $\Delta y_T \Delta y_R \ll \lambda\, d$, only one solution to the eigenfunction problems exists, corresponding to a plane wave that travels with direction from the transmit antenna to the receive antenna. Unfortunately, the result above by [44] is no longer valid when analyzing a LIS as the assumption of far apart antennas, and hence the parallax approximation typical of the Fraunhofer region, does not hold anymore.

The analytical derivation of the eigenfunctions and eigenvalues is in general elusive and one has to resort to e.m. simulations, which could be prohibitive for LISs and typically they do
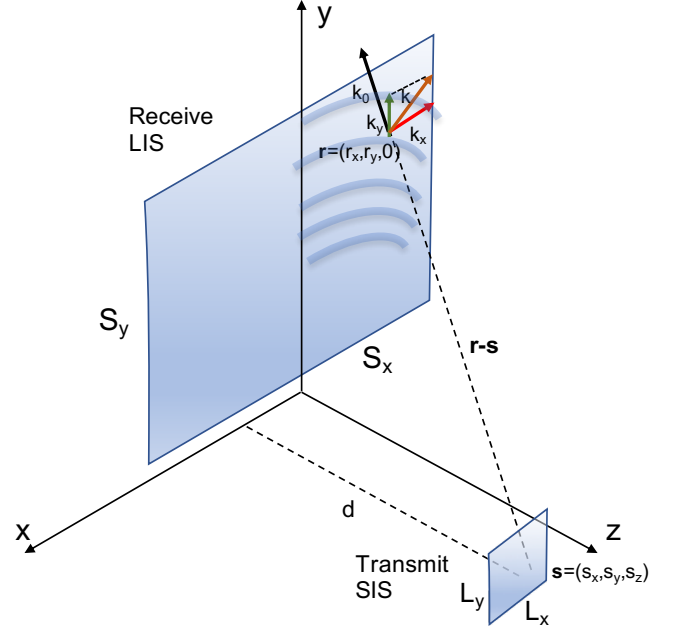

Fig. 3. Geometric configuration between SIS and LIS.

not provide general insights. In the next sections we bypass the direct derivation of the solutions to the eigenfunction problems by resorting to geometric arguments, with the purpose to determine the spatial DoF available for communication. Our aim is to derive simple expressions for particular geometric configurations of interest, also valid in the radiating near-field.

III. POWER GAIN BETWEEN LARGE AND SMALL-MEDIUM INTELLIGENT SURFACES

The coupling intensity for any generic geometric configuration of antennas can be easily computed by solving (16) numerically. Nevertheless, closed-form expressions can be obtained for some relevant cases from which interesting considerations can be derived.

Consider a transmit MIS/SIS and a receive LIS at distance d. This situation is expected to be common in practice where the MIS/SIS antenna might be embedded, for instance, into a smartphone or on top of a car, whereas the LIS coats a wall of a building (as in Fig. 1). Without loss of generality, the receive LIS is deployed along the xy-plane at $z = 0$, therefore the generic point on the surface is represented by the coordinates $\mathbf{r} = (r_x, r_y, 0) \in \mathcal{S}_R$ (see Fig. 3). Denote with $\mathbf{s} = (s_x, s_y, s_z) \in \mathcal{S}_T$ the coordinates of the generic point source of the transmit surface $\mathcal{S}_T$. The centers and sizes of the transmit and receive intelligent surfaces are, respectively, $\mathbf{s}_0 = (x_0, y_0, d)$, (L_x, L_y) and $\mathbf{r}_0 = (0, 0, 0)$, (S_x, S_y). The corresponding areas are $A_T = L_x L_y$ and $A_R = S_x S_y$. Since the transmit antenna is a MIS/SIS, it is reasonable to assume that $L_x, L_y \ll d$, $L_x \ll S_x$, and $L_y \ll S_y$. Contrarily, S_x and S_y may be of the same order of magnitude as d.

To calculate the link power gain between the transmit SIS and the receive LIS, one has to consider only the component of the power integrand in (16) perpendicular to the surface,

i.e.,

$$g = \frac{1}{\lambda^2} \int_{S_R} \int_{S_T} \frac{(r_y - s_y)^2 + (r_z - s_z)^2}{|\mathbf{r} - \mathbf{s}|^4} \hat{\mathbf{p}} \cdot \hat{\mathbf{n}} \, d\mathbf{r} \, d\mathbf{s}$$
$$\simeq \frac{A_T}{\lambda^2} \int_{S_R} \frac{((r_y - y_0)^2 + d^2) \, d}{|\mathbf{r} - \mathbf{s}_0|^5} \, d\mathbf{r}, \qquad (19)$$

where $\hat{\mathbf{p}} = (\mathbf{r} - \mathbf{s})/|\mathbf{r} - \mathbf{s}|$ is the direction of propagation, and $\hat{\mathbf{n}} = \hat{\mathbf{z}}$. In (19), we have made the approximations $s_z \simeq d$ and $|\mathbf{r} - \mathbf{s}|^2 \simeq |\mathbf{r} - \mathbf{s}_0|^2$, since the transmit antenna is small compared to the distance d. As a consequence, the result does not depend on SIS' orientation but only on its area A_T. Equation (19) can be solved in closed-form but the final expression is quite articulated and it does not provide important insights. Therefore, for the sake of space, we report here the result valid for $\mathbf{s}_0 = (0, 0, d)$ from which some interesting conclusions can be drawn. In this case, (19) becomes

$$g = \frac{A_T}{\lambda^2} \int_{-S_x/2}^{S_x/2} \int_{-S_y/2}^{S_y/2} \frac{d \left(r_y^2 + d^2 \right)}{\left(r_x^2 + r_y^2 + d^2 \right)^{5/2}} \, dr_x \, dr_y$$
$$= \frac{4d \, A_T S_x}{3\lambda^2} \int_{-S_y/2}^{S_y/2} \frac{6d^2 + S_x^2 + 6r_y^2}{\left(d^2 + r_y^2 \right) \left(4d^2 + S_x^2 + 4r_y^2 \right)^{3/2}} \, dr_y, \quad (20)$$

which gives

$$g = \frac{8A_T \left(\frac{S_x S_y d}{(S_x^2 + 4d^2)\sqrt{S_x^2 + S_y^2 + 4d^2}} + \tan^{-1} \left(\frac{S_x S_y}{2d\sqrt{S_x^2 + S_y^2 + 4d^2}} \right) \right)}{3\lambda^2}. \quad (21)$$

For a square LIS, the last expression simplifies as follows

$$g = \frac{4A_T}{3\lambda^2} \left(\frac{\sqrt{2}F}{\sqrt{1 + 2F}(1 + 4F)} + 2\mathrm{acot} \left(\sqrt{8F(1 + 2F)} \right) \right), \quad (22)$$

where $F = d^2/A_R$. It can be observed from (22) that the gain is a function of relative geometric quantities, i.e., the normalized (to the wavelength) transmit SIS' area A_T and the ratio F.

It is interesting to analyze the behavior of (22) when the LIS is extremely large compared to the distance d ($F \to 0$), that is

$$g^{\text{(large LIS)}} = \frac{4\pi A_T}{3\lambda^2}, \qquad (23)$$

which becomes independent of the distance. Instead, for large distances ($F \to \infty$), corresponding to the Fraunhofer far-field region, (22) gives

$$g^{\text{(large } d)} = \frac{A_T A_R}{\lambda^2 d^2}. \qquad (24)$$

The latter is the result found by Miller [44] (reported in (18) with a different normalization factor) when considering thin volumes and it is nothing else than the well-known Friis' formula. In fact, if one defines $G_I = \lambda^2/(4\pi d)^2$, $G_T = 4\pi A_T/\lambda^2$, and $G_R = 4\pi A_R/\lambda^2$, respectively, the isotropic free-space channel gain, the gain of the transmit and receive antennas considered as aperture antennas, it is $g^{\text{(large } d)} = G_T G_R G_I$ [47].

It is worth to notice that the comparison between (23) and (24) puts in evidence the limitation of classical path-loss formulas when using LISs. In fact, from (24) one could draw

the conclusion that by increasing the size of both the transmit and receive antenna it is possible to increase the link gain to any desired level. Instead, (23) tells that this is possible only up to a certain extent, i.e., until the size of one of the two antennas becomes very large so that the system works in the near-field region. In that region, the link gain is limited by the (normalized) area of the smallest of the two antennas. This result is a direct consequence of the diffraction effect of e.m. waves.

Equation (19) and, in particular, (21) and (22) represent simple design formulas useful to characterize the link budget in LIS-based communications without resorting to e.m. extensive simulations.

IV. COMMUNICATION DoF BETWEEN INTELLIGENT SURFACES

In this section we derive approximate expressions for the communication DoF between a transmit SIS and a receive LIS antenna following 2D sampling theory arguments. The accuracy of such expressions, with respect to the actual DoF value from the eigenfunction problems in Sec. II, is addressed in the numerical results.

With reference to Fig. 3, the wave originated by the point source $\mathbf{s}$ has wavenumber k_0 in the radial direction $\mathbf{r} - \mathbf{s}$ between the point source and the generic point $\mathbf{r}$ on the receive (observation) surface S_R. Contrarily to what happens in the 1D coordinate system, where a linear transformation never changes or generates new frequency components, when moving to 2D and 3D coordinate systems, it may happen that the observed wavenumber is different from k_0 if the observation direction is different from that of $\mathbf{r} - \mathbf{s}$. More specifically, along the x and y directions of the receive surface, the observed wave is characterized by wavenumber

$$\mathbf{k}(\mathbf{r}, \mathbf{s}) = k_0 \left(\hat{\mathbf{p}} - \hat{\mathbf{n}} (\hat{\mathbf{p}} \cdot \hat{\mathbf{n}}) \right) = (k_x(\mathbf{r}, \mathbf{s}), k_y(\mathbf{r}, \mathbf{s})), \quad (25)$$

where $\hat{\mathbf{p}} = (\mathbf{r} - \mathbf{s})/|\mathbf{r} - \mathbf{s}|$, and $\hat{\mathbf{n}}$ is the unit vector perpendicular to the surface in the point $\mathbf{r}$, so that

$$k_x(\mathbf{r}, \mathbf{s}) = k_0 \frac{r_x - s_x}{\sqrt{(r_x - s_x)^2 + (r_y - s_y)^2 + s_z^2}}$$
$$k_y(\mathbf{r}, \mathbf{s}) = k_0 \frac{r_y - s_y}{\sqrt{(r_x - s_x)^2 + (r_y - s_y)^2 + s_z^2}}. \quad (26)$$

Consider now an infinitesimal surface $d\mathbf{r}$ centered in $\mathbf{r}$. The received wave observed in $d\mathbf{r}$ can be seen as a two-dimensional signal whose local bandwidth changes slowly with $\mathbf{r} - \mathbf{s}$, and it is approximatively constant in $d\mathbf{r}$. The local bandwidth in the wavenumber domain observed in $d\mathbf{r}$ is the maximum wavenumber spread related to all point sources in S_T. Specifically it is

$$B(\mathbf{r}) = \frac{1}{4} \text{area} \left[\mathbf{k}(\mathbf{r}, \mathbf{s}) \right]_{\mathbf{s} \in S_T}, \qquad (27)$$

where the operator area$[\cdot]_{\mathbf{s} \in S_T}$ returns the area of the region in the complex plane spanned by the function $\mathbf{k}(\mathbf{r}, \mathbf{s})$ when parameter $\mathbf{s}$ varies in S_T.

Considering that the number of requested samples at Nyquist rate (i.e., the DoF) to represent a 2D signal of spatial

bandwidth B in an area S is equal to[4] $B\,S/\pi^2$, the DoF of the signal "projected" onto $\mathcal{S}_R$ results

$$D = \frac{1}{\pi^2} \int_{\mathcal{S}_R} B(\mathbf{r})\, d\mathbf{r}\,. \qquad (28)$$

In the next section we will make (28) particular to some LIS configurations with the purpose to derive simple expressions of the DoF and obtain some interesting insights.

A. DoF of Communicating Parallel LIS and SIS

For parallel intelligent surfaces, a way to compute (27) is to approximate the curve delimiting the area $[\mathbf{k}(\mathbf{r},\mathbf{s})]_{\mathbf{s}\in\mathcal{S}_T}$ with a quadrilateral having vertices given by $k_x^{(i)}(\mathbf{r}) = k_x\left(\mathbf{r},\mathbf{s}^{(i)}\right)$, $k_y^{(i)}(\mathbf{r}) = k_y\left(\mathbf{r},\mathbf{s}^{(i)}\right)$, $i = 1, 2, \ldots, 5$, with $\mathbf{s}^{(1)} = (x_0 - L_x/2, y_0 - L_y/2, d)$, $\mathbf{s}^{(2)} = (x_0 + L_x/2, y_0 - L_y/2, d)$, $\mathbf{s}^{(3)} = (x_0 - L_x/2, y_0 + L_y/2, d)$, $\mathbf{s}^{(4)} = (x_0 + L_x/2, y_0 + L_y/2, d)$, $\mathbf{s}^{(5)} = \mathbf{s}^{(1)}$, and then by applying the Gauss' formula

$$A(\mathbf{r}) \simeq \frac{1}{2}\left|\sum_{i=1}^{4}\left(k_x^{(i)}(\mathbf{r})\,k_y^{(i+1)}(\mathbf{r}) - k_x^{(i+1)}(\mathbf{r})\,k_y^{(i)}(\mathbf{r})\right)\right|\,. \qquad (29)$$

From (27), (28) and (29) it follows that

$$D^{\|} \simeq \frac{1}{4\pi^2} \int_{\mathcal{S}_R} A(\mathbf{r})\, d\mathbf{r}\,. \qquad (30)$$

Unfortunately, (30) does not admit a closed-form expression in general. However, even though it requires the evaluation of a two-folded integral, its numerical computation is very fast and it does not pose any particular issue compared to the numerical complexity of the eigenfunction problems (8) and (9).

Nevertheless, it could be of interest to derive closed-form expressions of (30) for some significant cases. Specifically, since $L_x, L_y \ll d$, setting $x_0 = y_0 = 0$, (30) gives (details are reported in Appendix B)

$$D^{\|} \simeq \frac{2L_x L_y}{\lambda^2}\left(\frac{S_x \tan^{-1}\left(\frac{S_y}{\sqrt{4d^2+S_x^2}}\right)}{\sqrt{4d^2+S_x^2}} + \frac{S_y \tan^{-1}\left(\frac{S_x}{\sqrt{4d^2+S_y^2}}\right)}{\sqrt{4d^2+S_y^2}}\right)\,. \qquad (31)$$

For $d \gg S_x, S_y$, i.e., in the far-field region, it is

$$D_{\text{large}}^{\|} = \frac{A_T A_R}{\lambda^2 d^2}\,, \qquad (32)$$

which gives (17) derived in [44].

The limit of (31) for $S_x, S_y \to \infty$, i.e., very large surfaces, is

$$D_{\text{asympt}}^{\|} = \frac{\pi\, L_x\, L_y}{\lambda^2} = \frac{\pi A_T}{\lambda^2}\,. \qquad (33)$$

Equation (33) indicates that the maximum DoF depends only on the area of the transmit surface (normalized to the square half-wavelength), i.e., the area of the smallest of the 2 antennas, and it represents the ultimate DoF limit which is independent of the distance. This result is reminiscent of

---

the DoF in MIMO systems when the channel matrix is full rank, i.e., in the presence of rich multipath [5]. Unfortunately, in LOS channel condition, the rank of the MIMO channel matrix is 1, and hence $D = 1$ (only beamforming gain is present). Instead, result (31) indicates that with a LIS one can obtain DoF larger than 1 even in LOS. Having large DoF in LOS could significantly increase the link capacity according to (15), especially at millimeter waves or in the THz band where the multipath is not rich or could be dominated by the LOS component.

B. DoF of Communicating Perpendicular LIS and SIS

Consider now a transmit surface along the plane xz with co-ordinates $\mathbf{s} = (s_x, y_0, s_z) \in \mathcal{S}_T$ and a perpendicular receive LIS at distance d with coordinates $\mathbf{r} = (r_x, r_y, 0) \in \mathcal{S}_R$. The centers and sizes of the transmit and receive intelligent surfaces are, respectively, $\mathbf{s}_0 = (x_0, y_0, d)$, (L_x, L_z) and $(0, 0, 0)$, (S_x, S_y). The corresponding areas are $A_T = L_x L_z$ and $A_R = S_x S_y$.

Following a similar approach as in Sec. IV-A, by setting $\mathbf{s}^{(1)} = (x_0 - L_x/2, y_0, d - L_z/2)$, $\mathbf{s}^{(2)} = (x_0 + L_x/2, y_0, d - L_z/2)$, $\mathbf{s}^{(3)} = (x_0 - L_x/2, y_0, d + L_z/2)$, $\mathbf{s}^{(4)} = (x_0 + L_x/2, y_0, d + L_z/2)$, it is

$$D^{\perp} \simeq \frac{2L_x L_z\left(\sqrt{4d^2+S_y^2}\cot^{-1}\left(\frac{2d}{S_x}\right) - 2d\tan^{-1}\left(\frac{S_x}{\sqrt{4d^2+S_y^2}}\right)\right)}{\lambda^2\sqrt{4d^2+S_y^2}}\,. \qquad (34)$$

For $d \gg S_x, S_y$ one gets

$$D_{\text{large}}^{\perp} = \frac{A_T A_R S_y}{4\lambda^2 d^3}\,, \qquad (35)$$

which, compared to (32) valid for parallel surfaces, denotes a dependence on the ratio S_y/d. Such a term contributes to increase the DoF when the LIS is tall and hence is capable to "see" better the transmit surface lying on the horizontal plane.

The limit of (34) for $S_x, S_y \to \infty$, i.e., very large surface, is

$$D_{\text{asympt}}^{\perp} = \frac{\pi A_T}{\lambda^2}\,, \qquad (36)$$

that is, the same as parallel surfaces.

V. NUMERICAL RESULTS

In this section, we present some numerical examples with the purpose to illustrate the potential advantages in communicating with LISs and to assess the validity of the method proposed to compute the DoF.

In Fig. 4, the link gain between a SIS communicating with a LIS using (21), normalized to $G_T = A_T\,4\pi/\lambda^2$, is shown as a function of F and for different values of LIS' aspect ratio $AR = S_x : S_y$. Notice that this plot does not depend on λ, on the absolute distance between the intelligent surfaces, and the dimension of the receive LIS, but only on the relative quantities $F = d^2/A_R$ and AR. When the size of the LIS is comparable or larger than the distance from the transmitter (small F), near-field effects become dominant leading to a saturation of the link gain toward the limit value (23). This can be ascribed to diffraction effects, which make the commonly
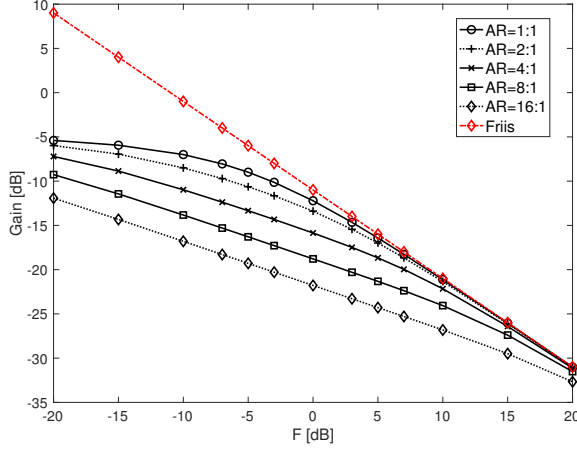
---

[4] Since a signal cannot be limited in both domains, this expression represents an approximation. An extensive discussion on this subject can be found in [50].

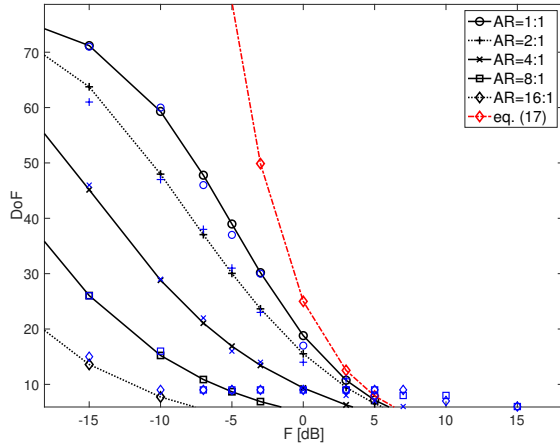Fig. 4. Normalized gain vs $F = d^2/A_R$ of a SIS-LIS link.

Fig. 5. DoF vs $F = d^2/A_R$ for parallel surfaces. $A_R = 25\,\text{cm}^2$, $f_c = 28\,\text{GHz}$. Blue markers refer to numerical solution to the eigenfunction problems.

Fig. 6. Amplitude of the x-component of eigenfunctions $\{\psi_n(\mathbf{r})\}$ (receive LIS).

Fig. 7. Phase of the x-component of eigenfunctions $\{\psi_n(\mathbf{r})\}$ (receive LIS).

used antenna aperture formula, according to which the antenna gain is proportional to the geometric area, no longer valid. From Fig. 4, it can also be noticed that the best geometric shape is the square one (AR = 1 : 1). For comparison, the gain obtained using the Friis' formula (24) is also shown, from which it is evident that it fails in modeling the link budget when LISs are used, especially for low F.

Now we investigate the DoF available when a LIS and a SIS are communicating in the near- and far-field. Fig. 5 shows the DoF in (31) related to parallel surfaces as a function of F for different values of AR, with $\lambda = 1\,\text{cm}$ ($f_c = 28\,\text{GHz}$), and $5 \times 5\,\text{cm}^2$ LIS ($A_T = 25\,\text{cm}^2$).[5]

For low F (very large LIS), the DoF saturates to the limit value given by (33), in this case equal to 78. As far as the Fraunhofer far-field regime is approached (large F), the DoF tends to one, as in conventional MIMO systems in LOS condition where only the beamforming gain is present.

[5]Although the values obtained from (31) should be rounded to the nearest integer value larger or equal to 1, here the continuous version is plotted to easy the reading.
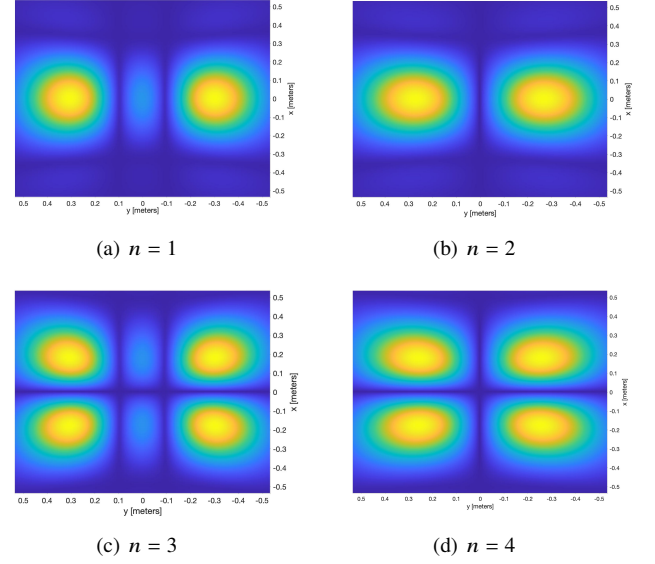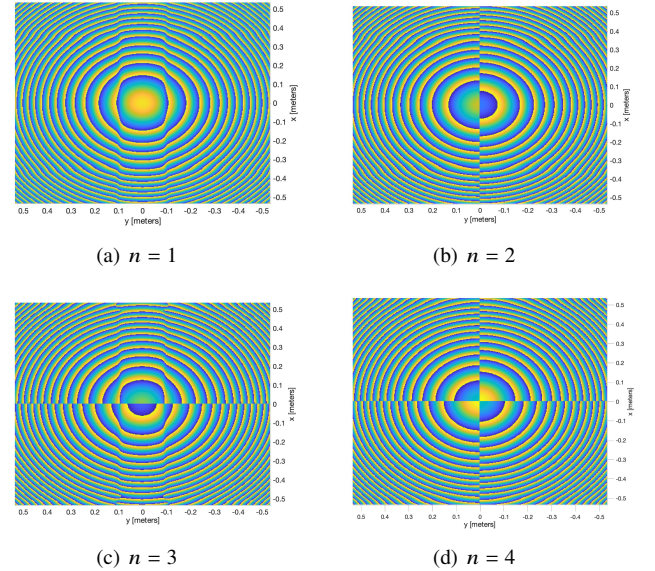
Again, the best LIS configuration is given by the square shape (AR = 1 : 1). The result obtained using (17) by [44] is also reported. It is evident how this expression, valid for antennas at distances much larger than their dimension, is not accurate for small F and it is not able to capture the effect of the aspect ratio of the LIS.

In order to validate the approach proposed in Sec. IV, results have been compared to those obtained by solving numerically the eigenfunction problems in Sec. II. To this purpose, different numerical approximation methods exist (e.g., Galerkin's method) [45]. Among them, we considered the following one: we decomposed each surface in very small square patches of side $\Delta = \lambda/16$ and we considered them as piece-wise constant basis functions for the surfaces. In this way, the eigenfunction problems can be approximated into a singular-

value decomposition problem with dimension $A_R/\Delta^2 \times A_T/\Delta^2$. Unfortunately, such a method becomes intractable as soon as the surfaces become large compared to λ due to the corresponding huge dimension of the matrix to decompose. To make the computation time affordable, we considered a MIS with $A_R = 1\,\mathrm{m}^2$. The DoF has been computed by considering the largest eigenvalues within a tolerance of 3 dB. Results are plotted in Fig. 5 (blue markers) and show a good agreement with the model developed in Sec. IV, especially for small F. For large F, there are some discrepancies, but the fact that our results are consistent with the analytical expression (17), which is accurate for large F, generates the suspect of numerical evaluation issues caused by the singular-value decomposition of huge likely ill-posed matrices.

To get a qualitative idea about the shape of the corresponding eigenfunctions, in Figs. 6-9 the amplitude and phase of the x-component of eigenfunctions $\{\psi_n(\mathbf{r})\}$, for $n = 1, 2, \ldots 4$, and $\{\phi_n(\mathbf{r})\}$, for $n = 1, 2$, are reported, respectively, under the same parameters used for the results in Fig. 5. For instance, Figs. 6a and 7a show the electric field observed at the receive LIS when the exciting current $\phi_1(\mathbf{r})$, corresponding to the largest coupling (i.e., the largest eigenvalue ξ_1^2) reported in Figs. 8a and 9a, is considered. From these figures one can notice that orthogonality does not involve in general non-overlapped waves. In fact, the received waves in Figs. 6a and 6b (or Figs. 6c and 6d) are almost overlapped, but the particular phase distribution deriving from the eigenfunction problems, reported in Fig. 7, guarantees the orthogonality between them. This means that classical beamforming or focusing schemes aiming at obtaining spatially non-overlapped waves are not in general optimal when using LISs. Similar considerations can be done with reference to the transmit SIS by observing Figs. 8a and 8b. Obviously, the generation of such eigenfunctions require a certain level of flexibility in the antenna configuration and signal processing capabilities which implies the adoption of dedicated architectures [20].

The DoF for perpendicular surfaces, given by (34), is reported in Fig. 10 as a function of F for different values of AR under the same conditions as that of Fig. 5. As it can be noticed, the achievable DoF is less than that obtained for parallel surfaces, which represents the best geometric configuration to maximize the DoF. It this case, the result in [44], reported in (17), is not applicable because it is not able to capture the DoF along the z direction of the SIS.

Interestingly, from the results in Figs. 5 and 10 it turns out that DoF significantly larger than 1 can be obtained at practical distances in LOS channel condition, which can have important implications in next generation wireless networks operating at millimeter wave and THz bands. For instance, suppose a typical industrial scenario is considered, where a LIS of size $5 \times 5\,\mathrm{m}^2$ is deployed on the factory ceiling at heigh $d = 5\,\mathrm{m}$. Supposing the transmitting sensors are equipped with SIS of area $A_T = 25\,\mathrm{cm}^2$ located close to the floor, from Fig. 5 it follows that the DoF is $D \simeq 20$ ($F = 0\,\mathrm{dB}$, AR = 1 : 1). This corresponds to a significant increase of link capacity with respect to the situation where only beamforming gain is exploited and $D = 1$. For instance, using (15), the capacity gain at SNR = 20 dB is about 7.76.
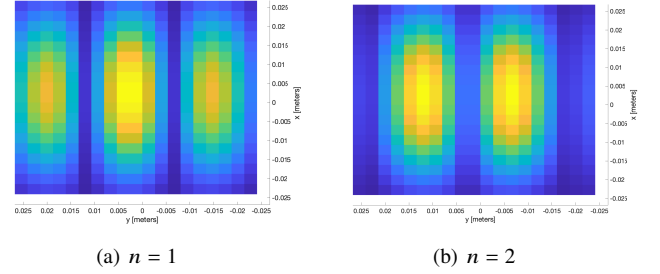

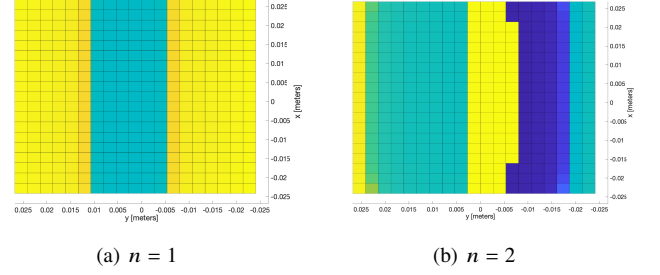Fig. 8. Amplitude of the x-component of eigenfunctions $\{\phi_n(\mathbf{r})\}$ (transmit SIS).

(a) $n = 1$ (b) $n = 2$

Fig. 9. Phase of the x-component of eigenfunctions $\{\phi_n(\mathbf{r})\}$ (transmit SIS).

(a) $n = 1$ (b) $n = 2$

This result can be interpreted also from another point of view: in fact, equivalently up to $D/A_T \simeq 8,000$ orthogonal links per square meter can be activated, which is very promising for the factories of the future where extremely high nodes densities are expected. In addition, the ability to create wireless links orthogonal at e.m. level, simplifies the channel multiple access, thus significantly reducing the communication latency.

VI. CONCLUSION

We have shown that the optimal communication between LIS/SIS can be formulated as an eigenfunctions problem starting from e.m. arguments. To obtain high-level descriptions of LIS-based communication and to avoid extensive and sometimes prohibitive e.m.-level simulations, simple but accurate analytical expressions for the link gain and the communication modes (i.e., DoF) between the transmitter and the receiver have been derived. The obtained expressions allow to get important insights about the communication between intelligent surfaces and can serve as design guidelines in future wireless networks employing LISs.

In particular, it has been shown that the achievable DoF and gain offered by the LIS-enabled wireless link are determined only by geometric factors normalized to the wavelength, and that the classical Friis' formula is no longer valid in this scenario. The fundamental limits for very large intelligent surfaces have been found to be dependent only on the normalized area of the smallest antenna involved in the communication.

Another important result is that using LISs one can exploit the spatial multiplexing even in LOS channel condition at practical distances, contrarily to conventional MIMO systems that can only exploit SNR enhancement (beamforming) when in strong LOS. This opens the possibility to satisfy the challenging requirements of next generation wireless networks
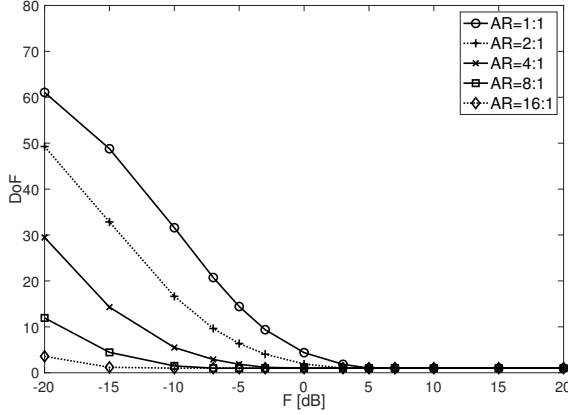
Fig. 10. DoF vs $F = d^2/A_R$ for perpendicular surfaces. $A_R = 25\,\text{cm}^2$, $f_c = 28\,\text{GHz}$.

operating at millimeter waves or THz bands in terms of massive communications and high capacity per square meter.

Obviously, several practical open issues need to be addressed before such limits can be approached by real systems. For instance, one fundamental research direction is the design of holographic metasurface technologies capable of approximating the eigenfunctions required to reach the fundamental limits with affordable complexity. Another issue, which deserves particular attention, is the definition of the regulatory power emission masks for LISs. In fact, the question is whether to define the emission masks at the whole antenna level, as done in current regulations with conventional antennas, or to define ad hoc emission masks, for instance, related to the effective radiated power (ERP) per square meter (ERP spatial density).

APPENDIX A

In this Appendix, we show that

$$\sum_n \xi_n^2 = \int_{S_R} \int_{S_T} ||G(\mathbf{r} - \mathbf{s})||^2 \, d\mathbf{r} \, d\mathbf{s}. \tag{37}$$

From (12), tensor $G(\mathbf{r} - \mathbf{s})$ allows the bilinear expansion

$$G(\mathbf{r} - \mathbf{s}) = \sum_n \xi_n \psi_n(\mathbf{r}) \otimes \phi_n^\dagger(\mathbf{s}). \tag{38}$$

The kjth element of tensor $G(\mathbf{r} - \mathbf{s})$ can be written as

$$\{G(\mathbf{r} - \mathbf{s})\}_{kj} = \sum_n \xi_n \, \{\psi_n(\mathbf{r})\}_k \cdot \{\phi_n^\dagger(\mathbf{s})\}_j, \tag{39}$$

then

$$\left|\{G(\mathbf{r} - \mathbf{s})\}_{kj}\right|^2 \tag{40}$$
$$= \sum_n \sum_m \xi_n \xi_m \, \{\psi_n(\mathbf{r})\}_k \, \{\psi_m^\dagger(\mathbf{r})\}_k \, \{\phi_n^\dagger(\mathbf{s})\}_j \, \{\phi_m(\mathbf{s})\}_j.$$

For each k it is

$$\sum_{j=1}^3 \left|\{G(\mathbf{r} - \mathbf{s})\}_{kj}\right|^2$$

$$= \sum_n \sum_m \xi_n \xi_m \, \{\psi_n(\mathbf{r})\}_k \, \{\psi_m^\dagger(\mathbf{r})\}_k \sum_{j=1}^3 \{\phi_n^\dagger(\mathbf{s})\}_j \, \{\phi_m(\mathbf{s})\}_j$$

$$= \sum_n \sum_m \xi_n \xi_m \, \{\psi_n(\mathbf{r})\}_k \, \{\psi_m^\dagger(\mathbf{r})\}_k \, \phi_n^\dagger(\mathbf{s}) \, \phi_m(\mathbf{s}). \tag{41}$$

By integrating in S_T with respect to $\mathbf{s}$ and thanks to the orthogonality condition (10), we obtain

$$\int_{S_T} \sum_{j=1}^3 \left|\{G(\mathbf{r} - \mathbf{s})\}_{kj}\right|^2 \, d\mathbf{s} = \sum_n \xi_n^2 \, \{\psi_n(\mathbf{r})\}_k \, \{\psi_n^\dagger(\mathbf{r})\}_k. \tag{42}$$

From the previous result, it follows that

$$\int_{S_T} ||G(\mathbf{r} - \mathbf{s})||^2 \, d\mathbf{s} = \int_{S_T} \sum_{k=1}^3 \sum_{j=1}^3 \left|\{G(\mathbf{r} - \mathbf{s})\}_{kj}\right|^2 \, d\mathbf{s}$$

$$= \sum_n \xi_n^2 \sum_{k=1}^3 \{\psi_n(\mathbf{r})\}_k \, \{\psi_n^\dagger(\mathbf{r})\}_k$$

$$= \sum_n \xi_n^2 \, |\psi_n(\mathbf{r})|^2. \tag{43}$$

By integrating (43) in S_R and exploiting again the orthogonality condition (10), we obtain the final result (37).

APPENDIX B

We show here the derivation of (31) from (30). Since $L_x, L_y \ll d$, setting $x_0 = y_0 = 0$, (30) can be expanded as

$$D \simeq \frac{k_0^2}{8\pi^2} \int_{-S_x/2}^{S_x/2} \int_{-S_y/2}^{S_y/2}$$

$$- \frac{U_x^-(r_x) \, U_y^+(r_y)}{\sqrt{\left((U_x^-(r_x))^2 + U_y^+(r_y))\right)^2 + d^2} \sqrt{(U_x^+(r_x))^2 + (U_y^+(r_y))^2 + d^2}}$$

$$+ \frac{U_x^+(r_x) \, U_y^+(r_y)}{\sqrt{(U_x^+(r_x))^2 + (U_y^+(r_y))^2 + d^2} \sqrt{(U_x^-(r_x))^2 + (U_y^+(r_y))^2 + d^2}}$$

$$- \frac{U_x^-(r_x) \, U_y^+(r_y)}{\sqrt{(U_x^-(r_x))^2 + (U_y^-(r_y))^2 + d^2} \sqrt{(U_x^-(r_x))^2 + (U_y^+(r_y))^2 + d^2}}$$

$$+ \frac{U_x^+(r_x) \, U_y^+(r_y)}{\sqrt{(U_x^+(r_x))^2 + (U_y^+(r_y))^2 + d^2} \sqrt{(U_x^+(r_x))^2 + (U_y^-(r_y))^2 + d^2}}$$

$$- \frac{U_x^+(r_x) \, U_y^-(r_y)}{\sqrt{(U_x^+(r_x))^2 + (U_y^+(r_y))^2 + d^2} \sqrt{(U_x^+(r_x))^2 + (U_y^-(r_y))^2 + d^2}}$$

$$+ \frac{U_x^-(r_x) \, U_y^-(r_y)}{\sqrt{(U_x^+(r_x))^2 + (U_y^-(r_y))^2 + d^2} \sqrt{(U_x^-(r_x))^2 + (U_y^-(r_y))^2 + d^2}}$$

$$+ \frac{U_x^-(r_x)\, U_y^-(r_y)}{\sqrt{(U_x^-(r_x))^2 + \left(U_y^+(r_y)\right)^2 + d^2}\sqrt{(U_x^-(r_x))^2 + \left(U_y^-(r_y)\right)^2 + d^2}}$$

$$- \frac{U_x^+(r_x)\, U_y^-(r_y)\, dr_x\, dr_y}{\sqrt{(U_x^+(r_x))^2 + \left(U_y^-(r_y)\right)^2 + d^2}\sqrt{(U_x^-(r_x))^2 + \left(U_y^-(r_y)\right)^2 + d^2}}\,, \tag{44}$$

where $U_x^+(r_x) = r_x + L_x/2$, $U_x^-(r_x) = r_x - L_x/2$, $U_y^+(r_y) = r_y + L_y/2$, and $U_y^-(r_y) = r_y - L_y/2$.

The integrand of (44) can be approximated with the first-order Taylor double series expansion in L_{x} and L_{y}

$$\frac{2d^2 L_{\mathrm{x}} L_{\mathrm{y}}}{\left(d^2 + r_x^2 + r_y^2\right)^2} + O\left(L_{\mathrm{x}}^2\right) + O\left(L_{\mathrm{y}}^2\right), \tag{45}$$

resulting in

$$D \simeq \frac{d^2 L_{\mathrm{x}} L_{\mathrm{y}}}{\lambda^2} \int_{-S_x/2}^{S_x/2} \int_{-S_y/2}^{S_y/2} \frac{1}{\left(d^2 + r_x^2 + r_y^2\right)^2}\, dr_x\, dr_y\,, \tag{46}$$

which admits a closed-form solution given by (31). Using similar arguments, a closed-form expression can be derived also for the more general case of $x_0, y_0 \neq 0$, but it is not reported here due to space constraints and also because no particular insights can be drawn from it.

REFERENCES

[1] S. Vitturi, C. Zunino, and T. Sauter, "Industrial communication systems and their future challenges: Next-generation ethernet, IIoT, and 5G," *Proceedings of the IEEE*, vol. 107, no. 6, pp. 944–961, June 2019.

[2] Z. Zhang, Y. Xiao, Z. Ma, M. Xiao, Z. Ding, X. Lei, G. K. Karagiannidis, and P. Fan, "6G wireless networks: Vision, requirements, architecture, and key technologies," *IEEE Vehicular Technology Magazine*, vol. 14, no. 3, pp. 28–41, Sep. 2019.

[3] E. Björnson, L. Sanguinetti, H. Wymeersch, J. Hoydis, and T. L. Marzetta, "Massive MIMO is a reality - what is next?: Five promising research directions for antenna arrays," *Digital Signal Processing*, 2019. [Online]. Available: http://www.sciencedirect.com/science/article/pii/S1051200419300776

[4] T. S. Rappaport, Y. Xing, O. Kanhere, S. Ju, A. Madanayake, S. Mandal, A. Alkhateeb, and G. C. Trichopoulos, "Wireless communications and applications above 100 GHz: Opportunities and challenges for 6G and beyond," *IEEE Access*, vol. 7, pp. 78 729–78 757, 2019.

[5] D. Tse and P. Viswanath, *Fundamentals of Wireless Communications*. New York, NY: Cambridge University Press, 2005.

[6] C. L. Holloway, E. F. Kuester, J. A. Gordon, J. O'Hara, J. Booth, and D. R. Smith, "An overview of the theory and applications of metasurfaces: The two-dimensional equivalents of metamaterials," *IEEE Antennas and Propagation Magazine*, vol. 54, no. 2, pp. 10–35, April 2012.

[7] S. B. Glybovski, S. A. Tretyakov, P. A. Belov, Y. S. Kivshar, and C. R. Simovski, "Metasurfaces: From microwaves to visible," *Physics Reports*, vol. 634, pp. 1 – 72, 2016. [Online]. Available: http://www.sciencedirect.com/science/article/pii/S0370157316300618

[8] I. A. Buriak, V. O. Zhurba, G. S. Vorobjov, V. R. Kulizhko, O. K. Kononov, and O. Rybalko, "Metamaterials: Theory, classification and application strategies (review)," *Journal of Nano- and Electronic Physics*, vol. 8, no. 4, 2016. [Online]. Available: https://search.proquest.com/docview/1853386963?accountid=9652

[9] L. Di Palma, A. Clemente, L. Dussopt, R. Sauleau, P. Potier, and P. Pouliguen, "Circularly-polarized reconfigurable transmitarray in Ka-band with beam scanning and polarization switching capabilities," *IEEE Transactions on Antennas and Propagation*, vol. 65, no. 2, pp. 529–540, Feb 2017.

[10] Y. Ra'di, V. S. Asadchy, and S. A. Tretyakov, "Tailoring reflections from thin composite metamirrors," *IEEE Transactions on Antennas and Propagation*, vol. 62, no. 7, pp. 3749–3760, July 2014.

[11] V. S. Asadchy, M. Albooyeh, S. N. Tcvetkova, A. Díaz-Rubio, Y. Ra'di, and S. A. Tretyakov, "Perfect control of reflection and refraction using spatially dispersive metasurfaces," *Phys. Rev. B*, vol. 94, p. 075142, Aug 2016. [Online]. Available: https://link.aps.org/doi/10.1103/PhysRevB.94.075142

[12] V. S. Asadchy, Y. Ra'di, J. Vehmas, and S. A. Tretyakov, "Functional metamirrors using bianisotropic elements," *Phys. Rev. Lett.*, vol. 114, p. 095503, Mar 2015. [Online]. Available: https://link.aps.org/doi/10.1103/PhysRevLett.114.095503

[13] S. V. Hum and J. Perruisseau-Carrier, "Reconfigurable reflectarrays and array lenses for dynamic antenna beam control: A review," *IEEE Transactions on Antennas and Propagation*, vol. 62, no. 1, pp. 183–198, Jan 2014.

[14] P. Nayeri, F. Yang, and A. Z. Elsherbeni, "Beam-scanning reflectarray antennas: A technical overview and state of the art." *IEEE Antennas and Propagation Magazine*, vol. 57, no. 4, pp. 32–47, Aug 2015.

[15] D. Dardari and D. Massari, "Using MetaPrisms for Performance Improvement in Wireless Communications," *arXiv e-prints*, p. arXiv:2003.13505, Mar. 2020.

[16] J. Hunt, J. Gollub, T. Driscoll, G. Lipworth, A. Mrozack, M. S. Reynolds, D. J. Brady, and D. R. Smith, "Metamaterial microwave holographic imaging system," *J. Opt. Soc. Am. A*, vol. 31, no. 10, pp. 2109–2119, Oct 2014. [Online]. Available: http://josaa.osa.org/abstract.cfm?URI=josaa-31-10-2109

[17] A. Silva, F. Monticone, G. Castaldi, V. Galdi, A. Alù, and N. Engheta, "Performing mathematical operations with metamaterials," *Science*, vol. 343, no. 6167, pp. 160–163, 2014. [Online]. Available: https://science.sciencemag.org/content/343/6167/160

[18] P. Nepa and A. Buffi, "Near-field-focused microwave antennas: Near-field shaping and implementation." *IEEE Antennas and Propagation Magazine*, vol. 59, no. 3, pp. 42–53, June 2017.

[19] D. Gonzlez-Ovejero, G. Minatti, G. Chattopadhyay, and S. Maci, "Multibeam by metasurface antennas," *IEEE Transactions on Antennas and Propagation*, vol. 65, no. 6, pp. 2923–2930, 2017.

[20] N. Shlezinger, O. Dicker, Y. C. Eldar, I. Yoo, M. F. Imani, and D. R. Smith, "Dynamic metasurface antennas for uplink massive MIMO systems," *IEEE Transactions on Communications*, vol. 67, no. 10, pp. 6829–6843, 2019.

[21] C. Liaskos, S. Nie, A. Tsioliaridou, A. Pitsillides, S. Ioannidis, and I. Akyildiz, "A new wireless communication paradigm through software-controlled metasurfaces," *IEEE Communications Magazine*, vol. 56, no. 9, pp. 162–169, Sep. 2018.

[22] M. Di Renzo and J. Song, "Reflection probability in wireless networks with metasurface-coated environmental objects: an approach based on random spatial processes," *EURASIP Journal on Wireless Communications and Networking*, vol. 2019, no. 1, p. 99, Apr 2019. [Online]. Available: https://doi.org/10.1186/s13638-019-1403-7

[23] M. D. Renzo, M. Debbah, D.-T. Phan-Huy, A. Zappone, M.-S. Alouini, C. Yuen, V. Sciancalepore, G. C. Alexandropoulos, J. Hoydis, H. Gacanin, J. d. Rosny, A. Bounceur, G. Lerosey, and M. Fink, "Smart radio environments empowered by reconfigurable AI meta-surfaces: an idea whose time has come," *EURASIP Journal on Wireless Communications and Networking*, vol. 2019, no. 1, p. 129, 2019. [Online]. Available: https://doi.org/10.1186/s13638-019-1438-9

[24] Y. Yang, S. Zhang, and R. Zhang, "IRS-enhanced OFDMA: Joint resource allocation and passive beamforming optimization," *IEEE Wireless Communications Letters*, pp. 1–1, 2020.

[25] S. Zhang and R. Zhang, "Capacity Characterization for Intelligent Reflecting Surface Aided MIMO Communication," *arXiv e-prints*, p. arXiv:1910.01573, Oct. 2019.

[26] Ö. Özdogan, E. Björnson, and E. G. Larsson, "Using Intelligent Reflecting Surfaces for Rank Improvement in MIMO Communications," *arXiv e-prints*, p. arXiv:2002.02182, Feb. 2020.

[27] K. Ntontin, M. Di Renzo, J. Song, F. Lazarakis, J. de Rosny, D. T. Phan-Huy, O. Simeone, R. Zhang, M. Debbah, G. Lerosey, M. Fink, S. Tretyakov, and S. Shamai, "Reconfigurable Intelligent Surfaces vs. Relaying: Differences, Similarities, and Performance Comparison," *arXiv e-prints*, p. arXiv:1908.08747, Aug 2019.

[28] J. Ye, S. Guo, and M.-S. Alouini, "Joint Reflecting and Precoding Designs for SER Minimization in Reconfigurable Intelligent Surfaces Assisted MIMO Systems," *arXiv e-prints*, p. arXiv:1906.11466, Jun. 2019.

[29] M. Jung, W. Saad, M. Debbah, and C. S. Hong, "On the Optimality of Reconfigurable Intelligent Surfaces (RISs): Passive Beamforming, Modulation, and Resource Allocation," *arXiv e-prints*, p. arXiv:1910.00968, Oct 2019.

[30] S. Hu, F. Rusek, and O. Edfors, "Beyond massive MIMO: The potential of data transmission with large intelligent surfaces," *IEEE Transactions on Signal Processing*, vol. 66, no. 10, pp. 2746–2758, May 2018.

[31] F. Guidi and D. Dardari, "Radio Positioning with EM Processing of the Spherical Wavefront," *arXiv e-prints*, p. arXiv:1912.13331, Dec. 2019.

[32] O. M. Bucci and G. Franceschetti, "On the degrees of freedom of scattered fields," *IEEE Transactions on Antennas and Propagation*, vol. 37, no. 7, pp. 918–926, July 1989.

[33] M. Franceschetti, M. D. Migliore, and P. Minero, "The capacity of wireless networks: Information-theoretic and physical limits," *IEEE Trans. Inf. Theor.*, vol. 55, no. 8, pp. 3413–3424, Aug. 2009. [Online]. Available: http://dx.doi.org/10.1109/TIT.2009.2023705

[34] M. Franceschetti, M. D. Migliore, P. Minero, and F. Schettino, "The degrees of freedom of wireless networks via cut-set integrals," *IEEE Transactions on Information Theory*, vol. 57, no. 5, pp. 3067–3079, May 2011.

[35] M. Franceschetti, *Wave Theory of Information*. Cambridge, UK: Cambridge University press, 2018.

[36] A. Pizzo, T. L. Marzetta, and L. Sanguinetti, "Spatially-Stationary Model for Holographic MIMO Small-Scale Fading," *arXiv e-prints*, p. arXiv:1911.04853, Nov. 2019.

[37] ——, "Degrees of Freedom of Holographic MIMO Channels," *arXiv e-prints*, p. arXiv:1911.07516, Nov. 2019.

[38] R. F. Harrington, *Time-Harmonic Electromagnetic Fields*. New York, USA: IEEE Press - Wiley, 2001.

[39] S. Hu, K. Chitti, F. Rusek, and O. Edfors, "User assignment with distributed large intelligent surface (LIS) systems," in *2018 IEEE 29th Annual International Symposium on Personal, Indoor and Mobile Radio Communications (PIMRC)*, Sep. 2018, pp. 1–6.

[40] A. Amiri, M. Angjelichinoski, E. de Carvalho, and R. W. Heath, "Extremely large aperture massive MIMO: Low complexity receiver architectures," in *2018 IEEE Globecom Workshops (GC Wkshps)*, Dec 2018, pp. 1–6.

[41] M. Jung, W. Saad, Y. Jang, G. Kong, and S. Choi, "Reliability analysis of large intelligent surfaces (LISs): Rate distribution and outage probability," *IEEE Wireless Communications Letters*, vol. 8, no. 6, pp. 1662–1666, 2019.

[42] ——, "Performance analysis of large intelligent surfaces (LISs): Asymptotic data rate and channel hardening effects," *IEEE Transactions on Wireless Communications*, vol. 19, no. 3, pp. 2052–2065, 2020.

[43] L. Zhang, X. Q. Chen, S. Liu, Q. Zhang, J. Zhao, J. Y. Dai, G. D. Bai, X. Wan, Q. Cheng, G. Castaldi, V. Galdi, and T. J. Cui, "Space-time-coding digital metasurfaces," *Nature Communications*, vol. 9, no. 1, p. 4334, 2018. [Online]. Available: https://doi.org/10.1038/s41467-018-06802-0

[44] D. A. B. Miller, "Communicating with waves between volumes: evaluating orthogonal spatial channels and limits on coupling strengths," *Appl. Opt.*, vol. 39, no. 11, pp. 1681–1699, Apr 2000. [Online]. Available: http://ao.osa.org/abstract.cfm?URI=ao-39-11-1681

[45] R. Piestun and D. A. B. Miller, "Electromagnetic degrees of freedom of an optical system," *J. Opt. Soc. Am. A*, vol. 17, no. 5, pp. 892–902, May 2000. [Online]. Available: http://josaa.osa.org/abstract.cfm?URI=josaa-17-5-892

[46] D. Dardari, "Communicating with intelligent surfaces," in *2020 IEEE International Conference on Communications (ICC): Communication Theory Symposium (IEEE ICC'20 - CT Symposium)*, Dublin, Ireland, Jun. 2020.

[47] C. A. Balanis, *Antenna Theory: analysis and design*. New Jersey, USA: Wiley, 2016.

[48] A. S. Y. Poon, R. W. Brodersen, and D. N. C. Tse, "Degrees of freedom in multiple-antenna channels: a signal space approach," *IEEE Transactions on Information Theory*, vol. 51, no. 2, pp. 523–536, Feb 2005.

[49] D. A. B. Miller, "Waves, modes, communications, and optics: a tutorial," *Adv. Opt. Photon.*, vol. 11, no. 3, pp. 679–825, Sep 2019. [Online]. Available: http://aop.osa.org/abstract.cfm?URI=aop-11-3-679

[50] D. Slepian, "Some comments on Fourier analysis, uncertainty and modeling," *SIAM Review*, vol. 25, no. 3, pp. 379–393, 1983. [Online]. Available: https://doi.org/10.1137/1025078